Stratospheric observations of noctilucent clouds: a new approach in studying middle- and large-scale mesospheric dynamics

Peter Dalin[1,2,*], Nikolay Pertsev[3], Vladimir Perminov[3], Denis Efremov[4,5], Vitaly Romejko[6]

[1] Swedish Institute of Space Physics, Box 812, SE-981 28 Kiruna, Sweden

[2] Space Research Institute, RAS, Profsouznaya st. 84/32, Moscow, 117997, Russia

[3] A.M. Obukhov Institute of Atmospheric Physics, RAS, Pyzhevskiy per. 3, Moscow, 119017, Russia

[4] Aerospace laboratory "Stratonautica", Moscow, Russia

[5] Faculty of Cosmic Research, M.V. Lomonosov Moscow State University, GSP-1, Leninskie Gory, Moscow, 119991, Russia

[6] The Moscow Association for NLC Research, Kosygina st. 17, Moscow, 119334, Russia

*Corresponding author at: Swedish Institute of Space Physics, Box 812, SE-981 28 Kiruna, Sweden. Fax: +46 980 79050. E-mail address: pdalin@irf.se (P. Dalin).

Abstract.

The experimental campaign Stratospheric Observations of Noctilucent Clouds (SONC) was conducted on the night of 5-6 July 2018 with the aim of photographing noctilucent clouds (NLCs) and studying their large-scale spatial dynamics at scales of 100–1450 km. An automated high-resolution camera (equipped with a wide-angle lens) was lifted by a stratospheric sounding balloon to 20.4 km altitude above the Moscow region in Russia (~56°N; 41°E), taking several hundreds of NLC images during the flight that lasted 1.7 hours. The combination of a high-resolution camera and large geographic coverage (~1500 km) have provided a unique technique of NLC observations from the stratosphere, which is impossible to currently achieve either from the ground or space. We have estimated that a horizontal extension of the NLC field as seen from the balloon was about 1450 x 750 km whereas it was about 800 x 550 km as seen from the ground. The NLC field was located in a cold area of the mesopause (136-146 K), which was confirmed by satellite measurements. The southmost edge of the NLC field was modulated by partial ice voids of 150-250 km in diameter. A medium-scale gravity wave had a wavelength of 49.4±2.2 km and amplitude of 1.9±0.1 km. The final state of the NLC evolution was represented by thin parallel gravity wave stripes. Balloon-borne observations provide new horizons in studies of NLCs at various scales from metres to thousands of km. Here we present a review paper on our experiment

34 describing initial results. Detailed studies on time evolution of the cloud movements will be done

35 in the future.

36

37 *Keywords*: noctilucent clouds, mesospheric dynamics, balloon-borne stratospheric

38 observations, atmospheric gravity waves

39

1 Introduction

41   Night-shining clouds or noctilucent clouds (NLCs) are the highest clouds in the Earth's

42 atmosphere observed at the summer mesopause between 80 and 90 km. NLCs can be readily

43 seen from mid- and subpolar latitudes of both hemispheres. NLCs are composed of water-ice

44 particles of 30–100 nm in radius that scatter sunlight and thus NLCs are observed against the

45 dark twilight arc from May until September in the Northern Hemisphere and from November

46 to February in the Southern Hemisphere (Bronshten and Grishin, 1970; Gadsden and

47 Schröder, 1989; Liu et al., 2016). NLCs are also observed from space and in this case they are

48 usually called Polar Mesospheric Clouds (PMCs) (Thomas, 1984).

49   NLCs are almost always represented by a wave surface having a complex interplay

50 between small-scale turbulence processes of 10-1000 metres, atmospheric gravity waves

51 (GW) with wavelengths of 10-1000 km, planetary waves, solar thermal tides and lunar

52 gravitational tides of about 10000 km (Witt, 1962; Fritts et al., 1993; Rapp et al., 2002;

53 Kirkwood and Stebel, 2003; Chandran et al., 2009; Dalin et al., 2010; Fiedler et al., 2011;

54 Taylor et al., 2011; Pertsev et al., 2015). Sometimes, distinguished non-linear mesospheric

55 phenomena like mesospheric walls or fronts appear at the mesopause which clearly separate

56 two volumes of the mesopause having cold and warm air masses with temperature difference

57 of 20-25 K across a few km (Dubietis et al., 2011; Dalin et al., 2013).

58   NLCs/PMCs are systematically observed and studied from the ground (optical imagers,

59 lidars), as well as from space (The Aeronomy of the Ice in the Mesosphere (AIM), Odin,

60 Solar Backscatter Ultraviolet Radiometer (SBUV) instruments) (e.g., Karlsson and Gumbel,

61 2005; Dalin et al., 2008; Bailey et al., 2009; Fiedler et al., 2011; DeLand and Thomas, 2015);

62 there are also irregular (campaign-based) NLC observations conducted by using sounding

63 rockets and aircraft (Zadorozhny et al., 1993; Gumbel and Witt, 2001; Reimuller et al., 2011).

64 These techniques have advantages and disadvantages. In particular, ground-based

65 measurements provide a high horizontal resolution of ~20 m and high temporal resolution of

66 seconds (optical imagers) (Dalin et al., 2010; Baumgarten and Fritts, 2014) and high vertical

67 resolution of 50-150 metres using lidars (Baumgarten et al., 2009) but are limited by

68 tropospheric weather conditions and restricted to a certain small region on the Earth's surface.

69 Satellite measurements, on the other hand, provide global PMC coverage but have low spatial

70 horizontal resolution (~5 km) as well as large spatial gaps of several hundreds of km between

71 adjacent orbits at middle and subpolar latitudes. Thus, there is no perfect technique to observe

72 and study NLCs/PMCs so far. At the same time, observations made from stratospheric

73 altitudes (20-40 km) are potentially available for comprehensive studies of NLCs/PMCs. So

74 far, there have been conducted three published experiments from stratospheric balloons

75 providing NLC/PMC observations. The first one was performed over Antarctica between 29

76 December 2012 and 9 January 2013 (Miller et al., 2015). The E and B Experiment (EBEX)

77 was dedicated to another research field concerning polarization in the cosmic microwave

78 background (Reichborn-Kjennerud et al., 2010). At the same time, two star cameras of the

79 EBEX experiment, having a narrow field of view of 4.1° x 2.7°, were able to register fine

80 structures of PMCs and turbulence dynamics, ranging from several km down to 10 m.

81 Another balloon-borne experiment (PMC-Turbo) was conducted between 8 and 14 July 2018

82 over Sweden-Greenland-Canada territories in order to capture NLCs with seven optical

83 cameras and lidar (Fritts et al., 2019). The PMC-Turbo experiment was launched about 2.5

84 days after the experiment described in the present paper.

85   In this paper, we report on scientific results of a new balloon-borne experiment dedicated

86 to studies of NLC middle- and large-scale dynamics at horizontal scales of more than 100 km

87 (Dalin et al., 2019). Such experiment, conducted for the first time, opens new horizons for

88 studies of middle- and large-scale dynamical features in combination with a high spatial

89 resolution at the summer mesopause, currently unachievable for other techniques like ground-

90 based and space measurements.

91

92 **2 Technique and method**

93   The Stratospheric Observations of Noctilucent Clouds (SONC) experiment is a special

94 balloon-borne experiment dedicated to studies of large-scale dynamical features in NLCs. A

95 high resolution high sensitive camera (Sony Alpha A7S), having a full frame 35 mm 12

96 megapixel sensor (4240 x 2832 pixels) and equipped with a wide-angle lens (field of view,

97 FoV, is 109.7° x 81.6°), has been installed on a meteorological sounding balloon. This

98 combination of a high resolution sensor and wide FoV yields spatial horizontal resolutions of

99 ~30 m and ~3000 m, when looking at 83 km from 20 km at elevation angles of 90° and 0°,

100 respectively. The horizontal coverage of a mesopause layer is over 2000 km, when viewing

101 along the horizon at low elevation angles. The balloon was launched from the Moscow

102 region, Russia (~56°N; 41°E), on the night of 5-6 July 2018. Since a gondola payload is

103 constantly rotating and shaking during its flight, the NLC camera was installed on a special

104 stabilized platform. The 3-axis motorized gimbal stabilized platform (Fig. 1) was designed

105 and built by the Aerospace laboratory "Stratonautica" (http://stratonautica.ru), which has a

106 wide experience in building such platforms and launching sounding balloons. The platform

107 was designed to rotate in a 60° step in the azimuth angle in order to capture the whole

108 hemisphere (360°) since NLCs can appear in any direction as observed from mid-latitudes,

109 including the southern part of the sky (Hultgren et al., 2011; Suzuki et al., 2016). The NLC

110 camera took images every 6 s during the whole flight, obtained several thousands of images

111 and several hundreds of images capturing NLCs. Besides, automatic exposure bracketing was

112 used to take four images in sequence with different exposures, allowing us to register various

113 NLC brightness from very bright to very faint as well as faint stars, which are important

114 information for the photogrammetric technique and georeference procedure of the images.

115 The balloon was launched at 21:34 UT on 5 July 2018 and the total flight duration was

116 about 1.7 hours. The ascent speed was around 5 m/s and the balloon reached its maximum

117 altitude of 20.4 km where it burst; then the payload descended with a parachute and the

118 payload was successfully recovered. A GPS receiver was installed onboard in order to obtain

119 information on the balloon trajectory. The flight characteristics of the SONC balloon are

120 shown in Fig. 2.

121 A ground-based support consisting of three automated NLC cameras was established in

122 the Moscow region in order to launch the balloon at the time of NLC appearance. Also, a

123 number of amateur observers significantly contributed to the NLC observational programme

124 before and during the flight. A launch window was preliminarily chosen at the beginning of

125 July based on long-term statistics of NLC observations conducted in the Moscow region since

126 1962 to present time. This statistics demonstrate that NLCs appear at the beginning of July

127 with about 65% occurrence probability on a clear night.

128

129 **3 The observation**

130 During the flight, the balloon-borne camera captured an extended NLC field with a

131 number of interesting features discussed in section 4. One can note the following general

132 characteristics of the NLC display:

133   a) NLCs were observed between 20:30 and 23:15 UT (23:30 and 02:15 LT) on 5 July

134 2018.

135   b) NLCs were located between 82.6 and 85.1 km. The NLC height was estimated by using

136 synchronously taken images obtained from two ground-based cameras located in the Moscow

137 region.

138   c) NLC field extended along the horizon from NW to NE at low elevation angles from –5°

139 to +11° as seen from the balloon.

140   d) NLCs were modulated by atmospheric gravity waves of various scales having

141 horizontal wavelength from 9 km to 50 km.

142   e) NLCs were traveling in a rather unusual direction from the south to north at the

143 observed mean speed of ~43 m/s.

144   f) NLCs were fading during the balloon ascent and they got very faint and less structured

145 at the maximum balloon altitude of 20.4 km. The brightest and well-developed NLCs were

146 observed when the SONC balloon was between 6 and 13 km, that is why we analyze the most

147 profound features of NLC images obtained at this height range.

148   Each analyzed NLC image was georeferenced using horizontal coordinates of referenced

149 stars (at least 15 stars are needed). The technique of the NLC georeference, triangulation

150 height estimation and error analysis can be found in Dalin et al. (2004, 2015).

151

152 **4 Results and discussion**

153   The projection of the NLC field on the surface along with the temperature map obtained

154 with the Aura/MLS spectrometer is shown in Fig. 3. The description on the MLS temperature

155 product and its validation can be found in Froidevaux et al. (2006) and Schwartz et al. (2008).

156 One can see that the NLC field (their actual coverage) extended mostly from the west to east

157 along an area filled with low temperatures of 136-146 K, and the NLCs were located north of

158 58°N due to rapidly increasing temperature with decreasing latitude. That is why the NLCs

159 were observed at low elevation angles (far to the north as seen from the Moscow region) on

160 this particular night.

161   Detailed analysis of five consecutive in time balloon-borne images (Figs. 4 and 5) has

162 revealed the following features of the NLC display:

163   a) The horizontal extent of the NLC field from the western to eastern observable border

164 was about 1450 km, and from the northern to southern border of about 750 km. Such

165 distances are impossible to observe from the ground due to the Earth's curvature and limited

166 area of the twilight arch. The central part of the NLC field, having extension of about 850 x

167   550 km, was seen from the ground but the western and eastern wings of the field as well as

168   the northern edge were located below the local ground horizon, making it impossible to

169   observe them. Thus, balloon-borne NLC observations have an obvious great advantage over

170   ground-based observations in terms of larger geographic coverage which is comparable to

171   PMC observations made from space since a PMC observation scene has spatial coverage of

172   about 2000 km along the AIM satellite track and 1000 km across track (Rusch et al., 2009).

173   b) The southmost edge of the NLC field was modulated by partial circles (something like

174   ice voids but with open southern border), whose centers are shown by the red arrows in

175   Figures 4 and 5. The diameters of these partial ice voids are estimated to be in the range of

176   150-250 km. The mechanism of the formation of ice voids in NLCs/PMCs is not clear now,

177   and it is an ongoing topic in atmospheric physics. One can mention three main mechanisms

178   which are currently discussing in the literature. Trubnikov and Skuratova (1967) addressed a

179   theory of cellular convection and demonstrated its principal possibility in the summer

180   mesosphere in relation to NLC occurrences. The authors estimated convective cells to be in

181   the range of 90-250 km in radius, that agrees well with sizes of partial ice voids obtained in

182   the present study. However, the main criterion for the convection to be developed, namely, the

183   height gradient of the potential temperature should have negative values. We have carefully

184   estimated the potential temperature gradient or the static stability (based on Aura/MLS

185   temperature measurements) in the analyzed area and could not find any signatures of its

186   negative values in the mesosphere and mesopause region. It means that in this particular case

187   cellular convection could not be responsible for the observed partial ice voids in the NLCs.

188   However, satellite measurements can easily miss a negative static stability at local scales

189   due to poor horizontal resolution and local ice voids may be generated by a gravity wave

190   breaking. Rusch et al. (2009) have hypothesized that ice voids could be caused by heating due

191   to the passage of warm crests of a gravity wave. It is possible in the present case. However,

192   we could not find any significant displacement of the partial ice voids (their boundaries)

193   relative to the NLC field, i.e., the partial ice voids traveled with the same speed and direction

194   as the entire NLC field did (~43 m/s from the south to north). One would expect an intrinsic

195   phase speed and intrinsic direction of the movement of the partial ice voids if they were

196   generated by a large-scale gravity wave of a wavelength of several hundreds of km. Thus, it is

197   difficult to prove this hypothesis of the influence of a large-scale gravity wave on the

198   formation of the observed partial ice voids.

199   Thurairajah et al. (2013b) have proposed another mechanism related to a shock wave

200   generated by a meteorite, which expands and cools the air that in turn leads to the formation

201 of large ice particles which fall out of an NLC field (analogously to hole-punch clouds due to

202 the passage of an aircraft). However, we observe large-scale partial ice voids (150-250 km) in

203 a broad area of the mesopause over 1000 km. It was hardly possible that any big meteorite

204 could produce such large holes in such broad area, and we did not observe any meteor motion

205 in our ground-based and balloon images.

206   Megner et al. (2018) have recently presented an interesting case study of a quasi-

207 stationary ice void in NLCs which did not follow the general wind, suggesting that it was

208 formed by a localized warming at the summer mesopause. This is not the case in our case

209 study, in which we have observed partial ice voids moving at the general wind speed in the

210 same direction along with the entire NLC field.

211   In the present case study, the partial ice voids had irregular shape and sizes ranging from

212 150 to 250 km. Also, these partial voids moved along the wind, having the same speed and

213 direction. Thus, it is difficult to connect these partial voids with regular wave disturbances. At

214 the same time, as shown in Fig. 3, the southmost border of the NLC field was confined to the

215 warm air mass located at sub-polar latitudes of ~58°N and lower. The mesopause temperature

216 at this border was equal to ~147 K at 86 km altitude. The MLS data cannot reproduce the

217 exact shape of this border due to low horizontal resolution (~15°) and temporal resolution of

218 ~1.5 h. However, it is well known that tropospheric frontal systems have a meandering shape,

219 sometimes with intrusions of warm and cold air masses as in case of the formation of a frontal

220 wave cyclone (Ahrens, 1993; Stull, 2000). In our case the warm front at the mesopause and

221 the NLC partial ice voids resemble a tropospheric frontal wave, in which there are intrusions

222 of warm air masses, moving from midlatitudes, into the cold air mass located at sub-polar and

223 polar latitudes (see Fig. 6). Therefore, we consider that the most probable source of these

224 partial ice voids observed in the NLCs in this particular case is the intrusion of warm air

225 masses into the cold air mass with the NLC field, sublimating ice particles. A similar

226 conclusion was proposed by Thurairajah et al. (2013a) who have analyzed a large ice void

227 observed in PMCs (using AIM/CIPS satellite images) and have concluded that "…*warmer*

228 *temperatures (warmer than the frost point temperature of ~144 K) at the location of the void*

229 *may be related to increased tidal activity and transport of warm air from low latitudes*." Also,

230 Rusch et al. (2009) and Thurairajah et al. (2013b) have demonstrated that southmost borders

231 of PMCs can be highly modulated by partial ice voids of several hundreds of km in diameter,

232 and the authors have found the structural similarity between PMC images and those seen in

233 tropospheric clouds.

234 c) Clear vertical modulation of the NLC layer is shown with the red arrow in Fig. 7. This is a

235 unique view on a particular gravity wave seen at the local horizon of the balloon; that is why

236 this wave modulation is viewed almost at the right angle to the line-of-sight. This geometry

237 allows observing a thin layer of NLC modulated in altitude by propagating gravity waves of

238 small and medium scales. Such geometry is almost impossible to obtain from the ground

239 since NLCs seen at the very horizon are usually masked by topography, tropospheric clouds

240 and, most importantly, by tropospheric aerosols, which are constantly present and

241 significantly absorb NLC brightness when looking at the very horizon. We have carefully

242 estimated parameters of this particular wave: its horizontal wavelength was equal to 49.4±2.2

243 km and its amplitude was 1.9±0.1 km. We define this amplitude as a semi-amplitude A of a

244 monochromatic wave with oscillation frequency ω, which is half of the peak-to-peak wave

245 amplitude between the highest (crest) and lowest (trough) displacement values. In this

246 calculation, the angle of 13.3° between the camera image plane and vertical plane at the NLC

247 altitude was taken into account. A unique altitude determination based on the balloon images

248 is possible under the assumption that the observed wave amplitude occurred in the vertical

249 plane only and due to the fact that the balloon traveled a small horizontal distance (about 2 m)

250 during a short exposure time of 1/8 s. Also note that since NLCs are clearly seen both in the

251 crest and trough of the wave (ice particles did not completely sublimated in the wave trough),

252 we have estimated the wave amplitude both in the wave crest and trough. The amplitude

253 estimations are the same in the wave trough and crest (within the given uncertainty). All this

254 makes us confident in the estimation of the amplitude of this particular wave. We have

255 analysed nine images at various viewing angles in order to deduce the maximum vertical

256 displacement (amplitude) of this particular wave. The nine images showing progressive

257 changes in the wave vertical displacement can be found at the following webpage:

258 ftp://ftp.irf.se/outgoing/pdalin/NLC/SONC_experiment_2018_07_05/WAVE_AMPLITUDE/

259 This is the most precise estimation of the amplitude of a gravity wave at the mesopause by

260 using NLC observations (Witt, 1962; Haurwitz and Fogle, 1969; Bronshten and Grishin,

261 1970; Demissie et al., 2014). Since wave amplitude represents wave energy per unit mass

262 (E~$0.5 \cdot A^2 \cdot \omega^2$), this is an important source of information for estimating the wave energy

263 budget at the upper atmosphere, and also can be used for future model studies to estimate a

264 wave source in the lower atmosphere (Demissie et al., 2014).

265   d) Small-scale billow-type gravity waves were estimated to have horizontal wavelengths

266 of 8-11 km (Fig. 7). Such small-scale gravity waves are well-known to be observed in NLC

267 layers (Witt, 1962; Dalin et al., 2010; Pautet et al., 2011; Baumgarten and Fritts, 2014;

268   Demissie et al., 2014), but we demonstrate this result in order to emphasize the ability to

269   resolve small-scale NLC structures by using a large FoV camera, having a high resolution

270   sensor, onboard a sounding balloon.

271   e) Figure 8 illustrates an NLC image taken from altitude of 20.3 km which is very close to

272   the maximum reached altitude of 20.4 km. The NLCs were rather faint by that time that is in

273   line with an idea of the intrusion of warm air masses from mid- to subpolar latitudes. These

274   large-scale warm air masses led to rapid sublimation of ice particles at large scales of about

275   1500 km. At the same time, on can see a very interesting feature to be considered. There were

276   several thin parallel gravity wave bands (stripes) with lengths of 50-200 km and widths of ~

277   3-5 km in cross-section. The reasons of seeing such thin stripes are as follows: (a) The SONC

278   balloon was in the stratosphere, i.e., above the troposphere in which optically strong air

279   turbulence is constantly present (b) The exposure time of this image was very short of 1/125 s.

280   All these made the image free from blurring (as minimum blurring as possible for moving

281   NLCs and balloon motion). This image demonstrates a final stage of the NLC evolution

282   (NLCs disappeared in 20 min since the image was taken), and these thin stripes might

283   represent a final morphological state of the NLC evolution. Further balloon-borne NLC

284   observations of very faint NLCs are required to confirm this consideration.

285

286   **5 Conclusions**

287   The combination of high resolution images (~30 m) and large geographic coverage (over

288   1500 km) is a unique property intrinsic to stratospheric balloon-borne NLC observations,

289   which is impossible to achieve either from the ground or space. In general, a balloon-borne

290   NLC observation provides us with the following new opportunities in case of a long duration

291   flight of several days:

292   a) NLC imaginary can be obtained for 24 hours a day and during several days due to very

293   little Rayleigh atmospheric scattering in the visible subrange of the spectrum above 20 km

294   (Hughes, 1964);

295   b) Quantitative information on a wide range of waves (gravity and planetary waves, solar

296   tides), propagating through the summer mesopause can be obtained;

297   c) Neutral wind velocity at the mesopause and large-scale trajectory of NLC fields over 1500

298   km can be measured;

299   d) Quantitative information on long mesospheric fronts, solitons and other non-linear

300   processes can be obtained;

301   e) Quantitative information on small-scale turbulent structures (down to 1 m) can be

302   obtained in case of using a narrow field of view lens.

303   f) High resolution vertical NLC structure (wave modulation, double layers) can be retrieved

304   by observing NLCs at the very horizon. Absence of any terrain obstacles and tropospheric

305   aerosol loading makes such stratospheric NLC observations unique.

306   g) Absence of optically strong tropospheric turbulence makes NLC images free from

307   atmospheric blurring that in turn results in well-defined fine structures of gravity waves

308   and turbulence in the mesopause region.

309

310   In the present study, we have estimated the following characteristics of the NLC field:

311   a) The horizontal extent of the NLC field as seen from the SONC balloon was about

312   1450 x 750 km whereas it was about 800 x 550 km as seen from the ground. This

313   emphasizes the great advantage of making large-scale balloon-borne observations over

314   medium-scale ground-based ones.

315   b) NLC field was traveling from the south to north at a mean velocity of 43 m/s;

316   c) The southmost edge of the NLC field was modulated by partial ice voids of 150-250

317   km in diameter, which were like generated by the intrusion of warm air masses

318   moving from mid- to sub-polar latitudes. The mesopause temperature at this edge was

319   equal to ~147 K, i.e., it was a threshold temperature separating the mesopause region

320   filled with NLCs from the warm area without NLCs.

321   d) A medium-scale wave had a wavelength of 49.4±2.2 km and vertical amplitude of

322   1.9±0.1 km. This is the most precise estimation of a gravity wave amplitude ever

323   made.

324   e) Small-scale billow-type gravity waves had wavelengths of 8-11 km.

325   f) The final morphology state of the NLC evolution was represented by thin parallel

326   gravity wave stripes with lengths of 50-200 km and widths of ~3-5 km.

327

328   *Data availability*. The reader can access the SONC experiment images and balloon GPS

329   coordinates, used in the paper, via publically available project ftp server at the Swedish

330   Institute of Space Physics:

331   ftp://ftp.irf.se/outgoing/pdalin/NLC/SONC_experiment_2018_07_05/

332

333 *Author contributions*. PD wrote the paper, made calculations and plotted the figures. NP and
334 VP read and made suggestions appropriated for the paper. DE provided the raw balloon-borne
335 images and balloon GPS coordinates. VR contributed to the image processing. All the authors
336 read and commented regarding the work and agreed with the content and submission of this
337 paper.
338
339 *Competing interests*. The authors declare that they have no conflict of interest.
340
341 *Acknowledgments*. The authors are grateful to Nikolay Gusev, Andrey Reshetnikov, Alexander
342 Dalin and Olga Dalina for their support of ground-based NLC observations during the SONC
343 experiment. The Aura/MLS data version 4.23 were obtained from the NASA Goddard Space
344 Flight Center Data and Information Services Center: https://mirador.gsfc.nasa.gov.
345
346 *Financial support*. The work was partly supported by the Russian Foundation for Basic
347 Research under project 15-05-04975a.
348

349 **References**

350 Ahrens, C. D.: Essentials of meteorology: an invitation to the atmosphere, West Publishing
351   Company, St. Paul, 1993.
352 Bailey, S. M., Thomas, G. E., Rusch, D. W., Merkel, A. W., Jeppesen, C., Carstens, et al.:
353   Phase functions of polar mesospheric cloud ice as observed by the CIPS instrument on the
354   AIM satellite, J. Atmos. Sol.-Terr. Phys., 71, 373–380,
355   http://dx.doi.org/10.1016/j.jastp.2008.09.039, 2009.
356 Baumgarten, G., Fiedler, J., Fricke, K. H., Gerding, M., Hervig, M., Hoffmann, P., et al.: The
357   noctilucent cloud (NLC) display during the ECOMA/MASS sounding rocket flights on 3
358   August 2007: morphology on global to local scales, Ann. Geophys., 27, 953–965, 2009.
359 Baumgarten, G., and Fritts, D. C.: Quantifying Kelvin-Helmholtz instability dynamics
360   observed in noctilucent clouds: 1. Methods and observations, J. Geophys. Res. Atmos.,
361   119, 9324–9337. doi:10.1002/2014JD021832, 2014.
362 Bronshten, V. A., and Grishin, N. I.: Noctilucent clouds, Nauka, Moscow, 1970.
363 Chandran, A., Rusch, D. W., Palo, S. E., Thomas, G. E., and Taylor, M. J.: Gravity wave
364   observations in the summertime polar mesosphere from the Cloud Imaging and Particle
365   Size (CIPS) experiment on the AIM spacecraft, J. Atmos. Sol.-Terr. Phys., 71, 392–400,
366   doi:10.1016/j.jastp.2008.09.041, 2009.

367 Dalin, P., Kirkwood, S., Moström, A., Stebel, K., Hoffmann, P., and Singer, W.: A case study
368   of gravity waves in noctilucent clouds, Ann. Geophys., 22, 1875-1884, 2004.

369 Dalin, P., Pertsev, N., Zadorozhny, A., Connors, M., Schofield, I., Shelton, I., et al.: Ground-
370   based observations of noctilucent clouds with a northern hemisphere network of
371   automated digital cameras, J. Atmos. Sol.-Terr. Phys., 70, 1460–1472, 2008.

372 Dalin, P., Pertsev, N., Frandsen, S., Hansen, O., Andersen, H., Dubietis, A., and Balciunas, R.:
373   A case study of the evolution of a Kelvin-Helmholtz wave and turbulence in noctilucent
374   clouds, J. Atmos. Sol.-Terr. Phys., 72,14-15, 1129-1138. doi:10.1016/j.jastp.2010.06.011,
375   2010.

376 Dalin, P., Connors, M., Schofield, I., Dubietis, A., Pertsev, N., Perminov, V., et al.: First
377   common volume ground-based and space measurements of the mesospheric front in
378   noctilucent clouds, Geophys. Res. Lett., 40, 6399–6404. doi:10.1002/2013GL058553,
379   2013.

380 Dalin, P., Pogoreltsev, A., Pertsev, N., Perminov, V., Shevchuk, N., Dubietis, A., et al.:
381   Evidence of the formation of noctilucent clouds due to propagation of an isolated gravity
382   wave caused by a tropospheric occluded front, Geophys. Res. Lett., 42, 2037-2046.
383   doi:10.1002/2014GL062776, 2015.

384 Dalin, P., Pertsev, N., Perminov, V., Efremov, D., and Romejko, V.: Looking at "night-
385   shining" clouds from the stratosphere, Eos, 100, https://doi.org/10.1029/2019EO118439,
386   2019.

387 DeLand, M. T., and Thomas, G. E.: Updated PMC trends derived from SBUV data, J.
388   Geophys. Res. Atmos., 120, 2140-2166, doi:10.1002/2014JD022253, 2015.

389 Demissie, T. D., Espy, P. J., Kleinknecht, N. H., Halten, M., Kaifler, N., and Baumgarten, G.:
390   Characteristics and sources of gravity waves observed in noctilucent cloud over Norway,
391   Atmos. Chem. Phys., 14, 12133–12142, doi:10.5194/acp-14-12133-2014, 2014.

392 Dubietis, A., Dalin, P., Balciunas, R., Cernis, K., Pertsev, N., Sukhodoev, V., et al.:
393   Noctilucent clouds: modern ground-based photographic observations by a digital camera
394   network, Applied Optics, 50, 28, F72-F79, doi:10.1364/AO.50.000F72, 2011.

395 Fiedler, J., Baumgarten, G., Berger, U., Hoffmann, P., Kaifler, N., and Lübken, F.-J.: NLC and
396   the background atmosphere above ALOMAR, Atmos. Chem. Phys., 11, 5701–5717,
397   doi:10.5194/acp-11-5701-2011, 2011.

398 Fritts, D. C., Isler, J. R., Thomas, G. E., and Andreassen, Ø.: Wave breaking signatures in
399   noctilucent clouds, Geophys. Res. Lett., 20, 2039–2042, doi:10.1029/93GL01982, 1993.

Fritts, D. C., and Alexander, M. J.: Gravity wave dynamics and effects in the middle atmosphere, Reviews of Geophysics, 41, 1003, doi:10.1029/2001RG000106, 2003.

Fritts, D. C., Miller, A.D., Kjellstrand, C.B., Geach, C., Williams, B.P., et al.: PMC Turbo: Studying gravity wave and instability dynamics in the summer mesosphere using polar mesospheric cloud imaging and profiling from a stratospheric balloon, J. Geophys. Res. Atmos., 124, https://doi.org/10.1029/2019JD030298, 2019.

Froidevaux, L., Livesey, N. J., Read, W. G., Jiang, Y. B., Jiménez, C. C., Filipiak, M. J., et al.: Early validation analyses of atmospheric profiles from EOS MLS on the Aura satellite, IEEE Transactions on Geoscience and Remote Sensing, 44, 5, 1106–1121, 2006.

Gadsden, M., and Schröder, W.: Noctilucent Clouds, Springer, New York, 1989.

Gumbel, J., and Witt, G.: Rocket-borne photometry of NLC particle populations, Adv. Space Res., 28, 7, 1053-1058, 2001.

Haurwitz, B., and Fogle, B.: Wave forms in noctilucent clouds, Deep-Sea Research, 16, 85-95, 1969.

Hemenway, C. L., Soberman, R. K., and Witt, G.: Sampling of noctilucent cloud particles, Tellus, XVI, 1, 84-88, 1964.

Hultgren, K., Körnich, H., Gumbel, J., Gerding, M., Hoffmann, P., Lossow, S., and Megner, L.: What caused the exceptional mid-latitudinal Noctilucent Cloud event in July 2009, J. Atmos. Sol.-Terr. Phys., 73, 2125-2131, 2011.

Hughes, J. V.: Sky brightness as a function of altitude, Applied Optics, 3, 10, 1135-1138, 1964.

Karlsson, B., and Gumbel, J.: Challenges in the limb retrieval of noctilucent cloud properties from Odin/OSIRIS, Adv. Space Res., 36, 935-942, doi:10.1016/j.asr.2005.04.074, 2005.

Kirkwood, S., and Stebel, K.: Influence of planetary waves on noctilucent clouds occurrence over NW Europe, J. Geophys. Res., 108, D8, 8440, doi:10.1029/2002JD002356, 2003.

Liu, X., Yue, J., Xu, J., Yuan, W., Russell III, J.M., Hervig, M. E., and Nakamura, T.: Persistent longitudinal variations in 8 years of CIPS/AIM polar mesospheric clouds, J. Geophys. Res. Atmos., 121, 8390–8409, doi:10.1002/2015JD024624, 2016.

Megner, L., Stegman, J., Pautet, P.-D., and Taylor, M. J.: First observed temporal development of a noctilucent cloud ice void, Geophys. Res. Lett., 45, https://doi.org/10.1029/2018GL078501, 2018.

Miller, A. D., Fritts, D. C., Chapman, D., Jones, G., Limon, M., Araujo, D., et al.: Stratospheric imaging of polar mesospheric clouds: a new window on small-scale

433   atmospheric dynamics, Geophys. Res. Lett., 42, 6058–6065, doi:10.1002/2015GL064758,

434   2015.

435 Pautet, P.-D., Stegman, J., Wrasse, C. M., Nielsen, K., Takahashi, H., Taylor, M. J., et al.:

436   Analysis of gravity waves structures visible in noctilucent cloud images, J. Atmos. Sol.-

437   Terr. Phys., 73, 14-15, 2082-2090, doi: 10.1016/j.jastp.2010.06.001, 2011.

438 Pertsev, N., Dalin, P., and Perminov, V.: Influence of semidiurnal and semimonthly lunar

439   tides on the mesopause as observed in hydroxyl layer and noctilucent clouds

440   characteristics, Geomagn. Aeron., 55, 6, 811–820, doi:10.1134/S0016793215060109,

441   2015.

442 Rapp, M., Lübken, F.-J., Müllemann, A., Thomas, G., and Jensen, E.: Small scale temperature

443   variations in the vicinity of NLC: experimental and model results, J. Geophys. Res., 107,

444   D19, 4392, doi:10.1029/2001JD001241, 2002.

445 Reichborn-Kjennerud, B., Aboobaker, A. M., Ade, P., Aubin, F., Baccigalupi, C., Bao, C., et

446   al.: EBEX: A balloon-borne CMB polarization experiment, Proceedings of SPIE,

447   Millimeter, Submillimeter and Far-Infrared Detectors and Instrumentation for Astronomy

448   V, San Diego, Calif., USA, 29 June–July 2010, Soc. of Photo-Opt. Instrum. Eng. (SPIE)

449   Conf. Ser., 7741, edited by W. S. Holland and J. Zmuidzinas, SPIE, Bellingham, Wash.

450   doi:10.1117/12.857138, 2010.

451 Reimuller, J. D., Thayer, J. P., Baumgarten, G., Chandran, A., Hulley, B., Rusch, D., Nielsen,

452   K., and Lumpe, J.: Synchronized imagery of noctilucent clouds at the day-night terminator

453   using airborne and spaceborne platforms, J. Atmos. Sol.-Terr. Phys., 73, 14-15, 2091-

454   2096, 2011.

455 Romejko, V. A., Dalin, P. A., and Pertsev, N. N.: Forty years of noctilucent cloud observations

456   near Moscow: database and simple statistics, J. Geophys. Res. Atmos., 108, D8, 8443,

457   doi:10.1029/2002JD002364, 2003.

458 Rusch, D. W., Thomas, G. E., McClintock, W., Merkel, A. W., Bailey, S. M., Russell III, J. M.,

459   Randall, C. E., Jeppesen, C., Callan, M.: The cloud imaging and particle size experiment

460   on the aeronomy of ice in the mesosphere mission: cloud morphology for the northern

461   2007 season, J. Atmos. Sol.-Terr. Phys., 71, 356–364, 2009.

462 Schwartz, M. J., Lambert, A., Manney, G. L., Read, W. G., Livesey, N. J., Froidevaux, L., et

463   al.: Validation of the Aura Microwave Limb Sounder temperature and geopotential height

464   measurements, J. Geophys. Res., 113, D15S11, 2008.

465 Stull, R. B.: Meteorology for scientists and engineers, Second Edition, Brooks/Cole, Pacific

466   Grove, 2000.

467 Suzuki, H., Sakanoi, K., Nishitani, N., Ogawa, T., Ejiri, M. K., Kubota, M., Kinoshita, T.,
468   Murayama, Y., and Fujiyoshi, Y.: First imaging and identification of a noctilucent cloud
469   from multiple sites in Hokkaido (43.2–44.4°N), Japan, Earth, Planets and Space, 68, 182,
470   DOI 10.1186/s40623-016-0562-6, 2016.

471 Taylor, M. J., Pautet, P.-D., Zhao,Y., Randall, C. E., Lumpe, J., Bailey, S. M., et al.: High-
472   latitude gravity wave measurements in noctilucent clouds and polar mesospheric clouds.
473   In: Abdu M., Pancheva, D. (eds), Aeronomy of the Earth's Atmosphere and Ionosphere,
474   IAGA Special Sopron Book Series, Springer, Dordrecht, 2, 93-105, doi:10.1007/978-94-
475   007-0326-1_7, 2011.

476 Thomas, G. E.: Solar Mesosphere Explorer measurements of polar mesospheric clouds
477   (noctilucent clouds), J. Atmos. Terr. Phys., 46, 9, 819-824, 1984.

478 Thurairajah, B., Bailey, S. M., Siskind, D. E., Randall, C. E., Taylor, M. J., and Russell III, J.
479   M.: Case study of an ice void structure in polar mesospheric clouds, J. Atmos. Sol.-Terr.
480   Phys., 104, 224-233, http://dx.doi.org/10.1016/j.jastp.2013.02.001, 2013a.

481 Thurairajah, B., Bailey, S. M., Nielsen, K., Randall, C. E., Lumpe, J., Taylor, M. J., and
482   Russell III, J. M.: Morphology of polar mesospheric clouds as seen from space, J. Atmos.
483   Sol.-Terr. Phys., 104, 234-243, http://dx.doi.org/ 10.1016/j/jastp.2012.09.009, 2013b.

484 Trubnikov, B. N., and Skuratova, I. S.: Cellular convection in the zone of noctilucent clouds,
485   Proceedings of the International Symposium on Noctilucent Clouds, Tallinn, 1966, 208-
486   215, Eds. I.A. Khvostikov and G. Witt, VINITI, Moscow, 1967.

487 Witt, G.: Height, structure and displacements of noctilucent clouds, Tellus, 14, 1, 1–18, 1962.

488 Zadorozhny, A. M., Tyutin, A. A., Witt, G., Wilhelm, N., Wälchli, U., Cho, J. Y. N., and
489 Swartz, W. E.: Electric field measurements in the vicinity of noctilucent clouds and PMSE,
490 Geophys. Res. Lett., 20, 20, 2299-2302, 1993.

491 **Figure captions:**

492 **Figure 1**. The 3-axis motorized gimbal stabilized platform, holding the NLC camera,

493 designed and built by the Aerospace laboratory "Stratonautica". Photo by Denis Efremov.

494

495 **Figure. 2**. (Left) the altitude of the SONC balloon as a function of time flight. (Right) the

496 vertical-horizontal trajectories of the SONC balloon: the red line is the upleg and the black

497 line is the downleg trajectory.

498

499 **Figure 3**. The temperature map at the mesopause (geometric height of 86.1 km) as measured

500 by the Aura/MLS spectrometer on 5 July 2018. Nighttime measurements around the globe

501 have been selected to produce the map. Upon the temperature map, the outer borders of the

502 NLC field (the actual NLC coverage) are overplotted: the red line is as seen from the SONC

503 balloon, the black line is as seen from the ground at the launch. The black dots mark the

504 position of the balloon at 7.8 km at the ground and ground-based observers.

505

506 **Figure 4**. The NLC field as observed from the SONC balloon at 4092 m, 4947 m, 7836 m,

507 9077 m and 13928 m above the ground at 21:46 UT, 21:49 UT, 21:57 UT, 22:01 UT, 22:20

508 UT on 5 July 2018. The red arrows indicate the centers of large areas free from NLC particles

509 (partial ice voids).

510

511 **Figure 5**. Projection of the NLC fields (shown in Figure 4) as observed from the SONC

512 balloon on the surface. The red arrows indicate the centers of large areas free from NLC

513 particles (partial ice voids).

514

515 **Figure 6.** A schematic representation of the intrusion of warm air masses from mid- to sub-

516 polar latitudes, forming partial ice voids in the observed NLCs. A general concept of this

517 scheme is analogous to the formation of a wave cyclone in the troposphere (see Figs. 8.18 and

518 8.19 in Ahrens, 1993).

519

520 **Figure 7.** The SONC balloon image taken at 6222 m above the ground at 21:49 UT on 5 July

521 2018. The red arrow marks the vertical modulation of the NLC layer by a gravity wave of

522 medium scale. The green arrow indicates small-scale billow-type gravity waves.

523

524 **Figure 8**. The SONC balloon image taken at 20.3 km above the ground at 22:48 UT on 5 July

525 2018 represents the final stage of NLC evolution on that night.

526

527
Figure 1. The 3-axis motorized gimbal stabilized platform, holding the NLC camera,
designed and built by the Aerospace laboratory "Stratonautica". Photo by Denis Efremov.

530
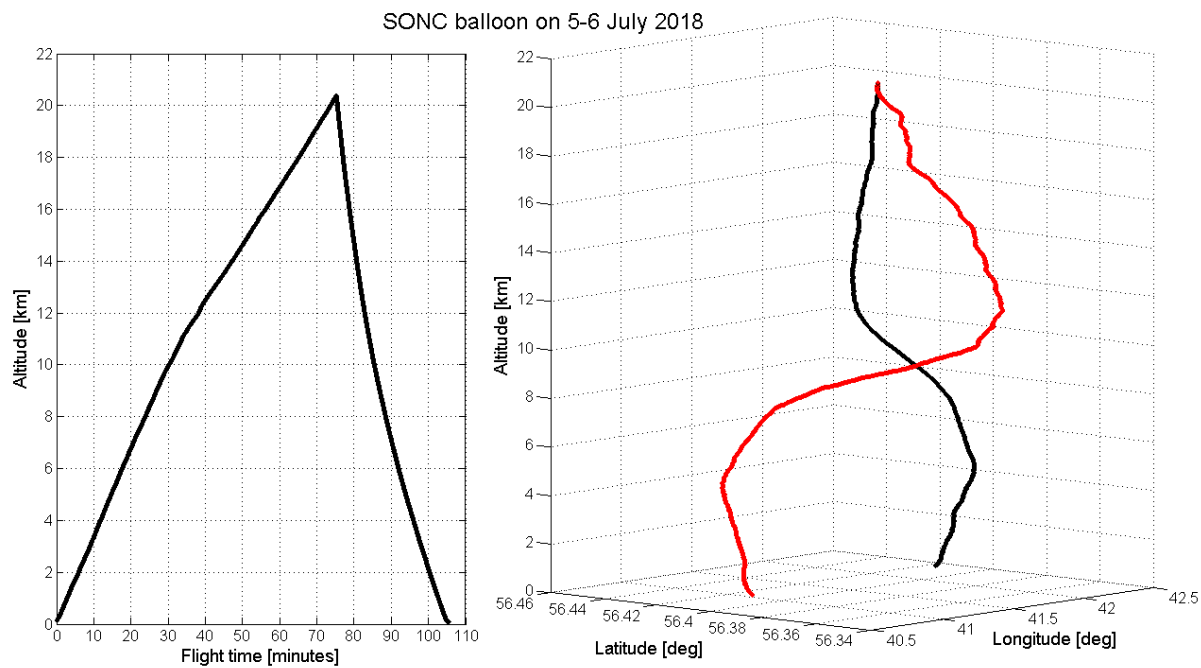
Figure. 2. (Left) the altitude of the SONC balloon as a function of time flight. (Right) the vertical-horizontal trajectories of the SONC balloon: the red line is the upleg and the black line is the downleg trajectory.
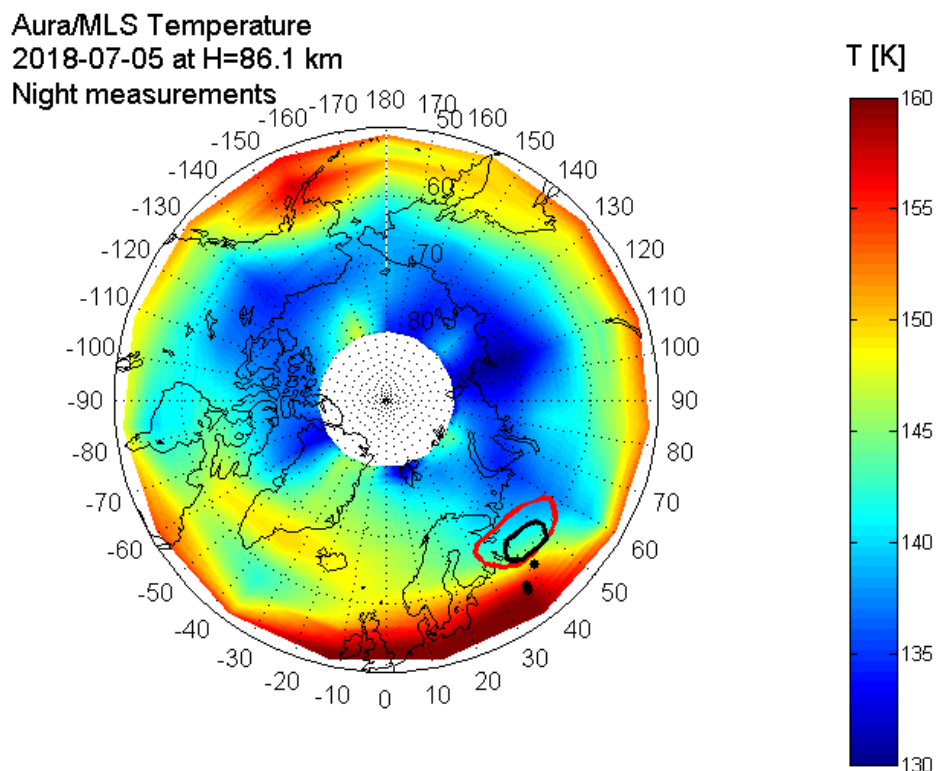
536

537 **Figure 3**. The temperature map at the mesopause (geometric height of 86.1 km) as measured

538 by the Aura/MLS spectrometer on 5 July 2018. Nighttime measurements around the globe

539 have been selected to produce the map. Upon the temperature map, the outer borders of the

540 NLC field are overplotted: the red line is as seen from the SONC balloon, the black line is as

541 seen from the ground at the launch. The black dots mark the position of the balloon at 7.8 km

542 at the ground and ground-based observers.

543

544

545 **Figure 4**. The NLC field as observed from the SONC balloon at 4092 m, 4947 m, 7836 m,
546 9077 m and 13928 m above the ground at 21:46 UT, 21:49 UT, 21:57 UT, 22:01 UT, 22:20
547 UT on 5 July 2018. The red arrows indicate the centers of large areas free from NLC particles
548 (partial ice voids).
549

550
551
552
553
554
555
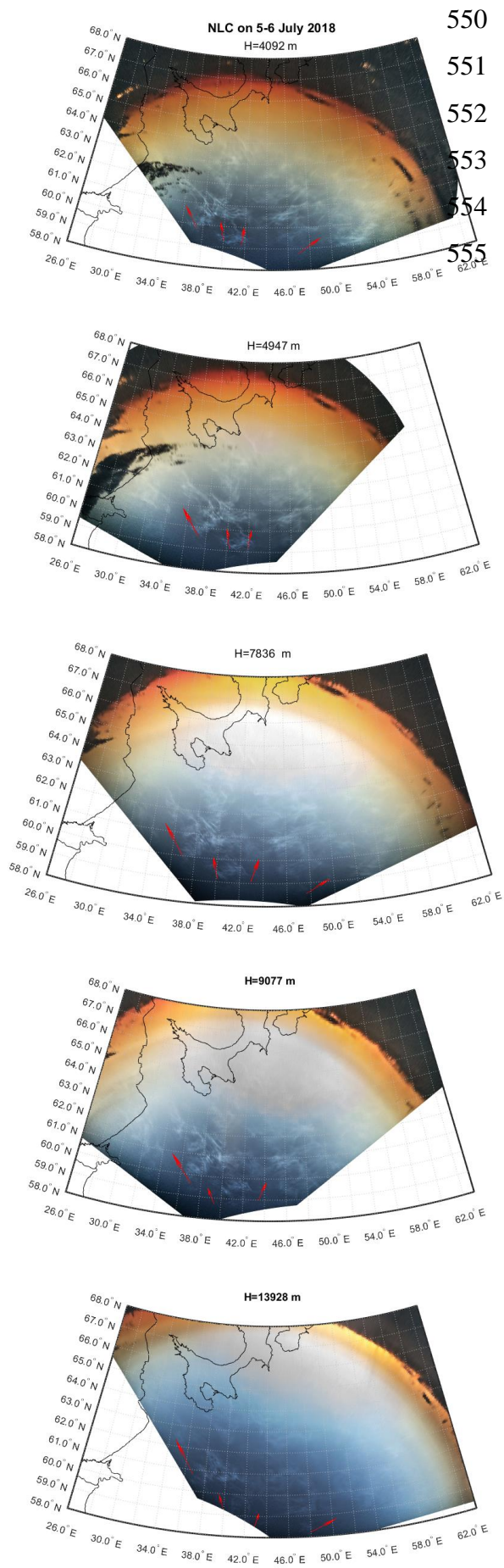
Figure 5. Projection of the NLC fields (shown in Figure 4) as observed from the SONC balloon on the surface. The red arrows indicate the centers of large areas free from NLC particles (partial ice voids).
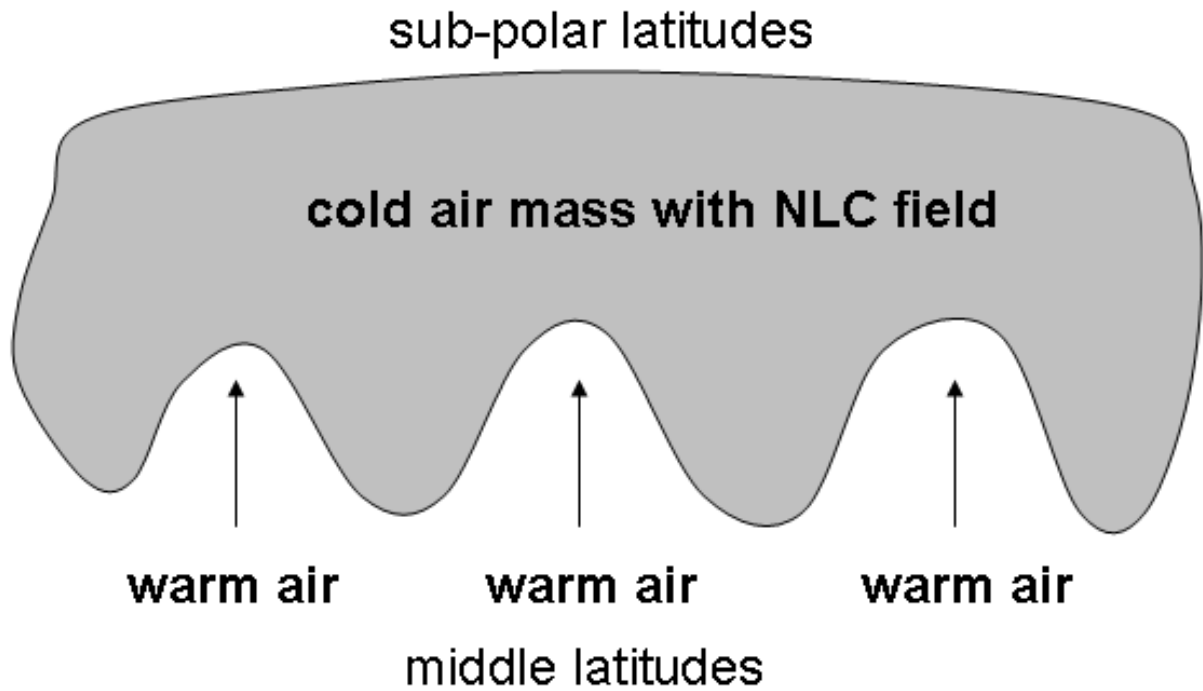
556

Figure 6. A schematic representation of the intrusion of warm air masses from mid- to sub-
polar latitudes, forming partial ice voids in the observed NLC. A general concept of this
scheme is analogous to the formation of a wave cyclone in the troposphere (see Figs. 8.18 and
8.19 in Ahrens, 1993).

Figure 7. The SONC balloon image taken at 6222 m above the ground at 21:49 UT on 5 July 2018. The red arrow marks the vertical modulation of the NLC layer by a gravity wave of medium scale. The green arrow indicates small-scale billow-type gravity waves.

Figure 8. The SONC balloon image taken at 20.3 km above the ground at 22:48 UT on 5 July 2018 represents the final stage of NLC evolution on that night.